EBW simulation for MAST and NSTX experiments

J. Preinhaelter[1)], G. Taylor[2)], V. Shevchenko[3)], J. Urban[1)], M. Valovic[3)], P. Pavlo[1)], L. Vahala[4)], G. Vahala[5]

1) EURATOM/IPP.CR Association, Institute of Plasma Physics, 182 21 Prague, Czech Republic

2) Princeton Plasma Physics Laboratory, Princeton, New Jersey 08543, USA

3) EURATOM/UKAEA Fusion Association, Culham Science Centre, Abingdon, OX14 3DB, UK

4) Old Dominion University, Norfolk, VA 23529, USA

5) College of William & Mary, Williamsburg, VA 23185, USA

This work was partially funded by the United Kingdom Engineering and Physical Sciences Research Council, by EURATOM, by U.S. Dept. of Energy by AS CR project #AV0Z-20430508..

.

EBW in spherical tokamaks

- The **low magnetic field** and **high plasma density** in a spherical tokamak **do not permit** the usual radiation of **O and X modes** from the first five electron cyclotron harmonics
- **only electron Bernstein modes** (unaffected by any density limits) - **converted into the electromagnetic waves in the upper hybrid resonance region** - can be responsible for the measured radiation

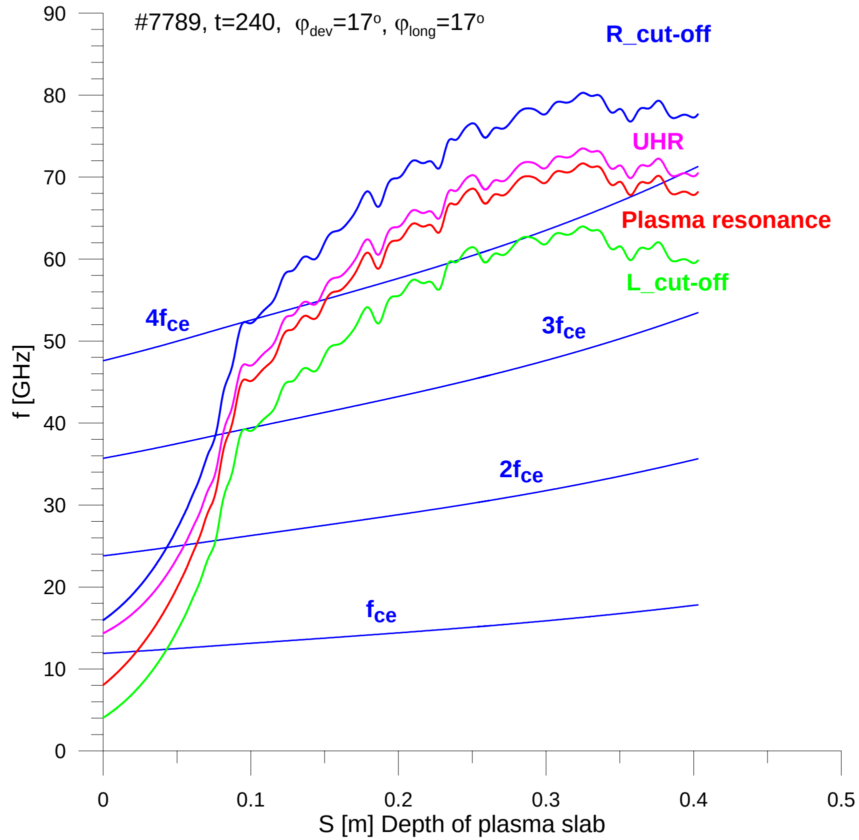

Cutoffs and resonances in MAST cold plasma for normal incidence

MAST and NSTX ECE antenna systems

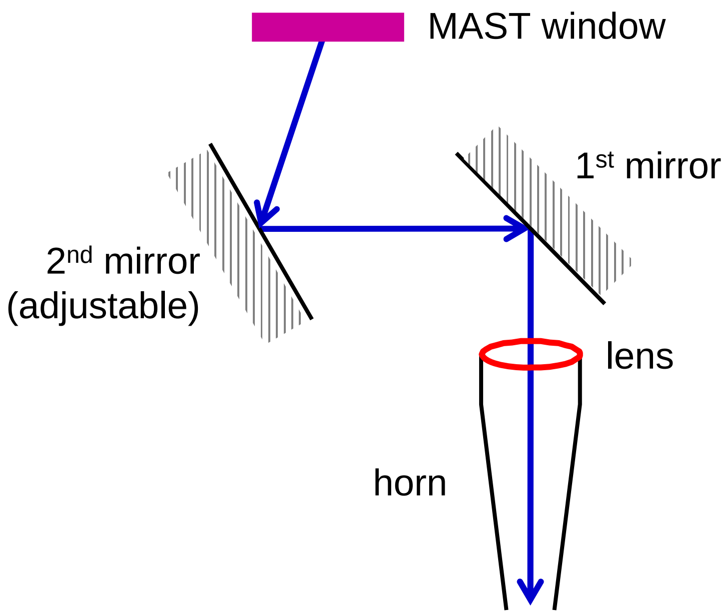

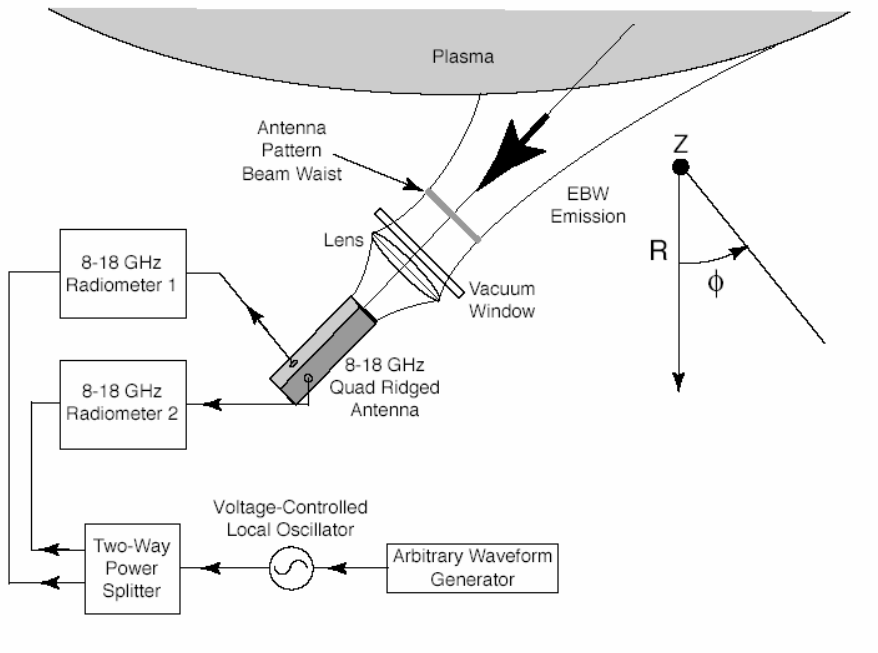

- Both antenna are described in the frame of the Gaussian beam theory
- EBW emission is determined by integrating the contributions of the individual rays over the waist in front of plasma
- EBW emission from MAST is transmitted only by those rays which go through the window and are not blocked by the vessel wall

3D spherical tokamak plasma model

- A realistic 3D model of the MAST plasma has been developed for the simulation
- The magnetic field is reconstructed by splining of the two potentials determined by the EFIT code, assuming toroidal symmetry
- The temperature and density profile are obtained from the Thomson scattering measurements, beyond the LCFS exponentially decaying profiles are used

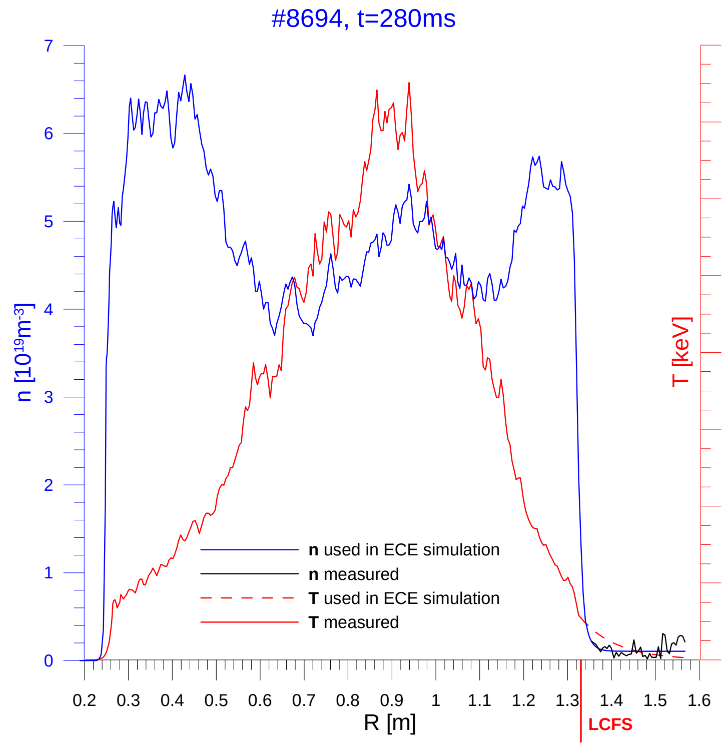

← density, electron temperature profiles

magnetic surfaces

ψ(R,Z) →

MAST shot #8694, t= 280ms

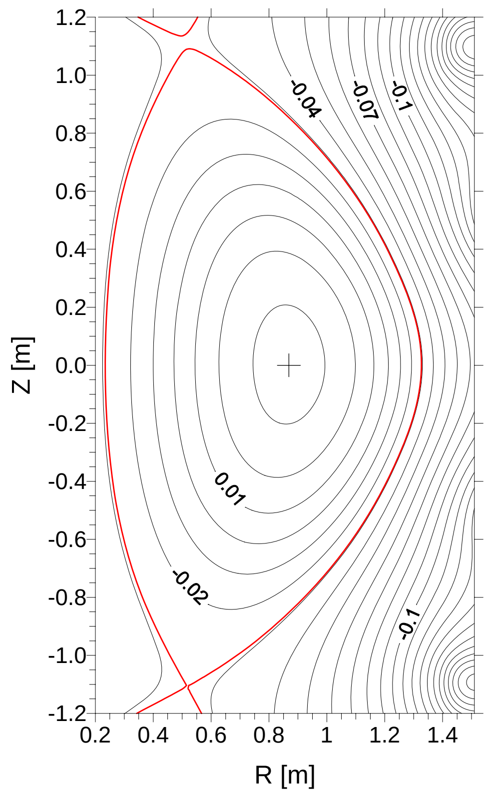

The Gaussian beam is replaced by rays

- Intersection of the antenna beam with the LCFS (last closed flux surface) determines the position of the spot

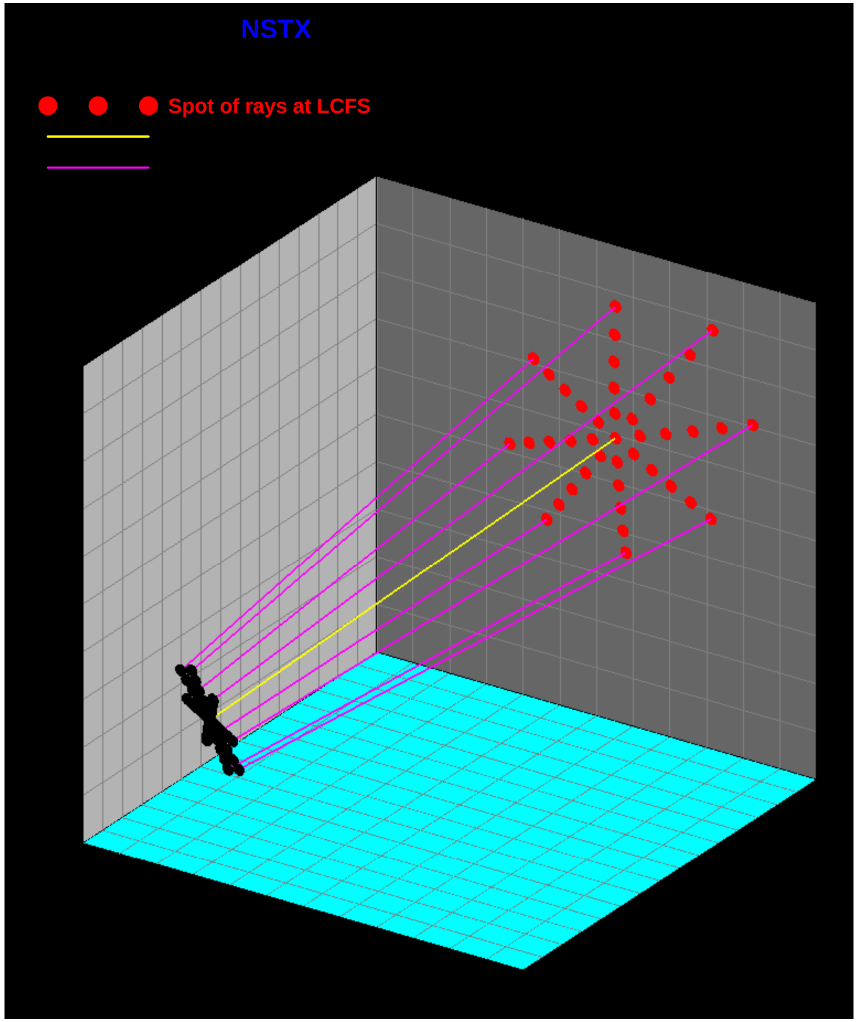

Plane stratified slab and mode conversion efficiency estimation

- Full wave solution of Maxwell's equations in the cold plasma slab is used for determination of the EBW-X-O conversion efficiency

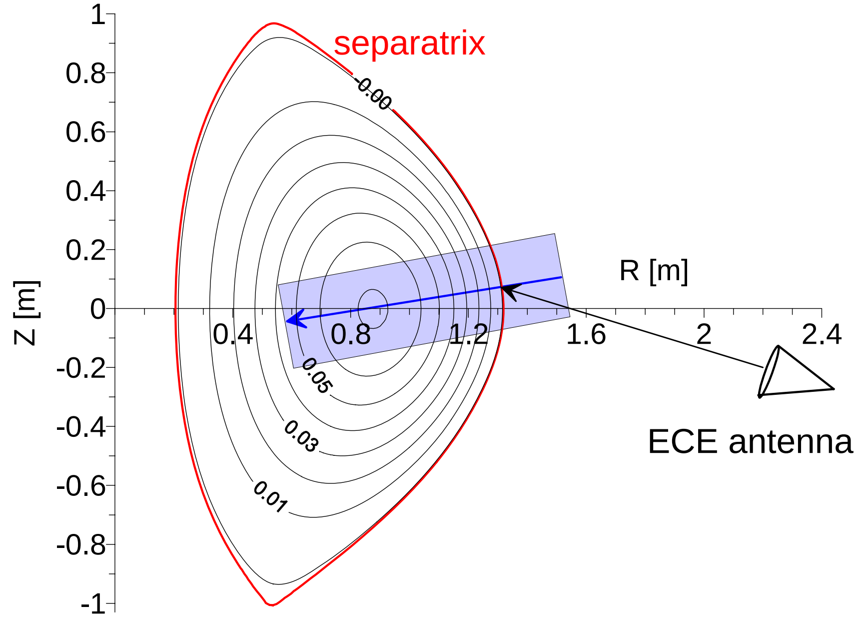

Conversion efficiency using the adaptive finite elements method

- The 2nd order ODE's in the cold plasma model are solved assuming weak collisions
- The absorbed power in the UHR equals the power of the converted EBW
- Adaptive mesh is refined in regions of large local errors

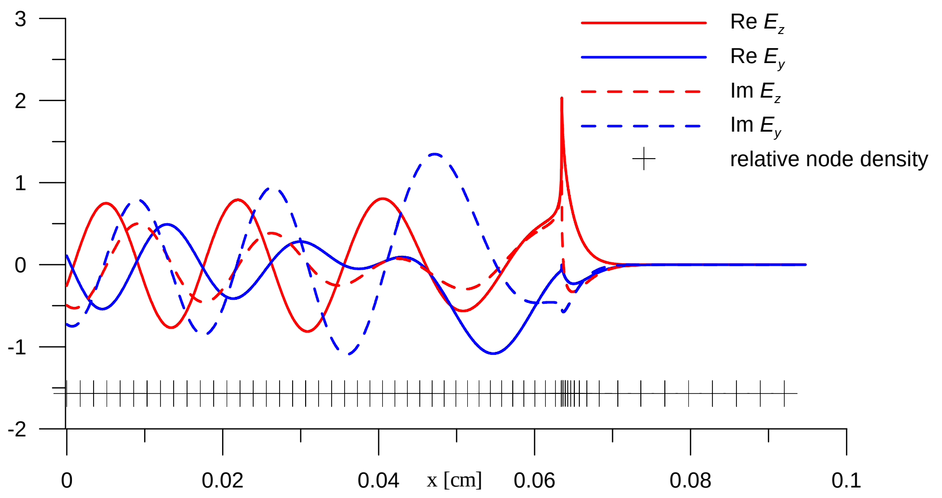

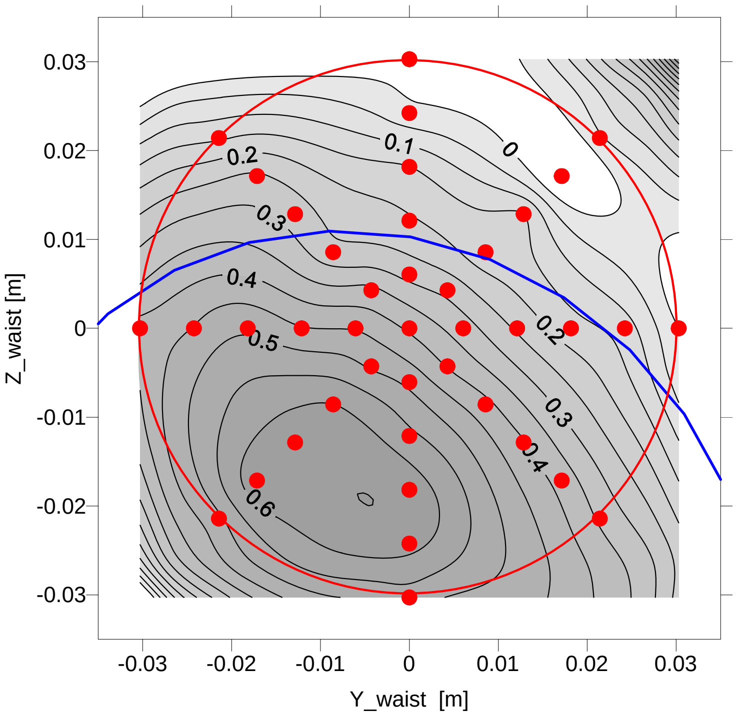

Sample contour map of the conversion efficiency projected to the waist plane

The red dots represent individual rays, the blue line is the projection of the MAST window rim

Ray-tracing

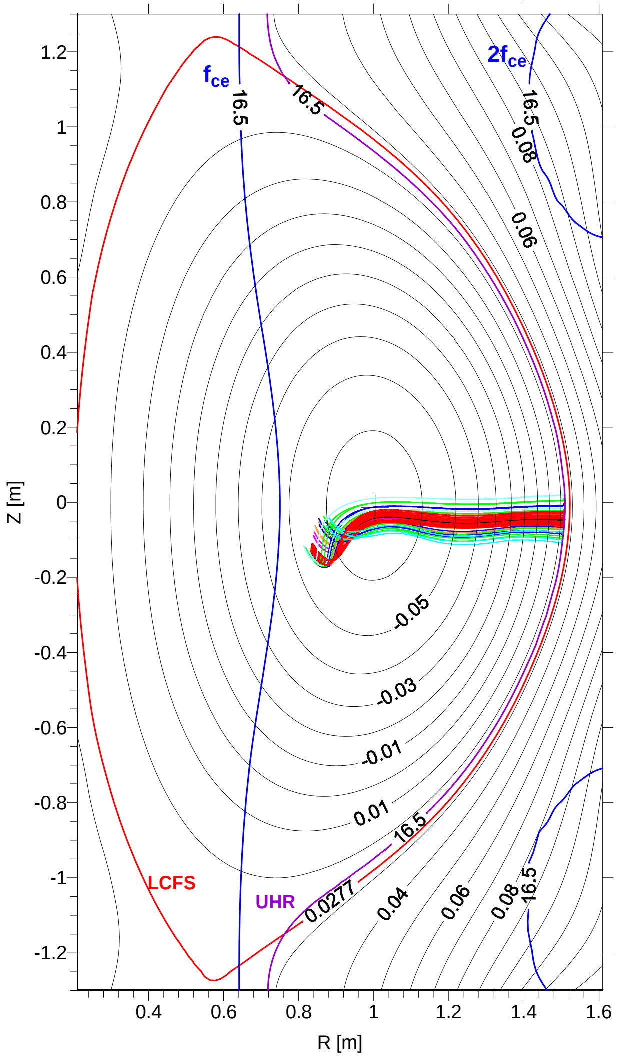

- A ray-tracing code is used to determine the radiation temperature from the Rayleigh-Jeans law
- The rays with Z~0 propagate in **NSTX** deep into the plasma and are absorbed close to the first electron cyclotron harmonic (f=16,5GHz, #113544, t=0.325s)

Radiative temperature and EBW absorption

- Ray equations describe the motion of EBW packet ➔ the evolution equation for the power has to be integrated simultaneously with the ray
  $dP/dt=-2\gamma(t)P$
- Non-local reabsorption of the radiation is described by the radiative transfer equation
  $dP/dt=\eta-\alpha P$
  which must be solved simultaneously with the ray evolution equation
- The emitted power can be expressed by the Rayleigh-Jeans law with T_{rad} instead of local temperature T
  $P \sim \omega^2 T_{rad}$
  where
  $T_{rad}= {}_0\int^{\infty} 2\gamma(t')T(t')\, \exp\{-{}_0\int^{t'} 2\gamma(t'')dt''\}dt'$

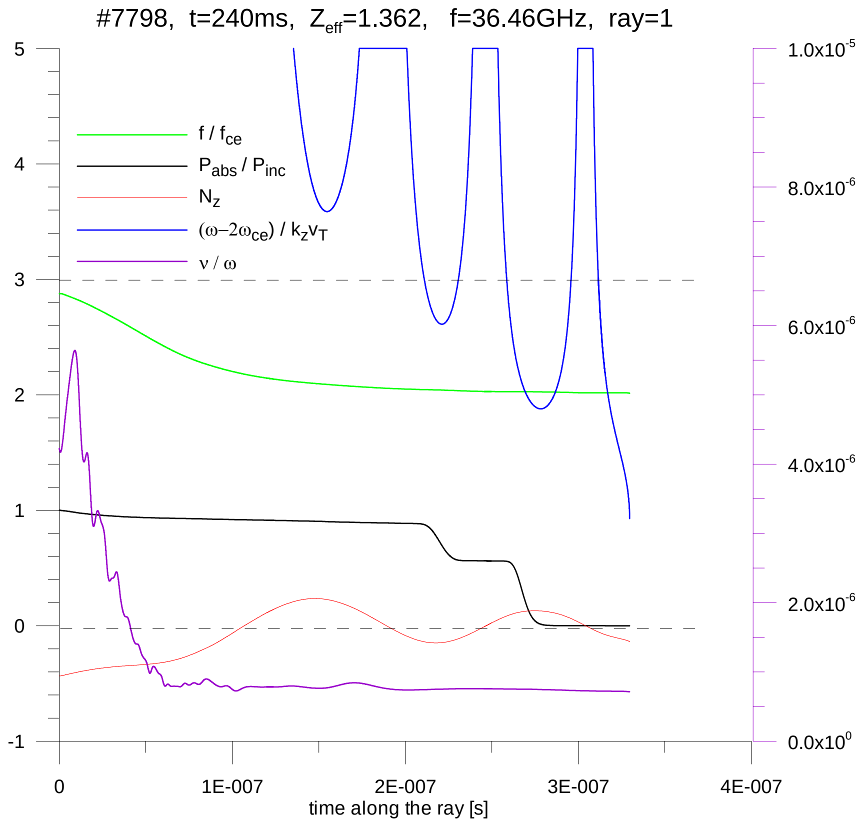

ECE intensity

- The intensity of ECE detected by the antenna can be expressed as

$$I_{ECE} = const \times \iint \mathrm{d}S\, W_{Gauss} C_{EBW-X-O} \omega^2 T_{rad} C_{window} V_{relat}$$

where

$W_{Gauss} = e^{-\left(2r^2 / w_0^2\right)}$ - Gaussian weight (w_0 is the waist radius)

$C_{EBW-X-O}$ - conversion efficiency

$\omega^2 T$ - Rayleigh-Jeans black body radiation law

C_{window} - power transmission coefficient of the MAST window

$V_{relat} = w^2 / w_0^2$ - relative visible area (w is the Gaussian beam radius at the plasma surface)

- The integration is taken over the intersection of the waist and the projection of the vessel window rim

Simulation of EBW emission in MAST

- Our model of EBW emission gives good fit with observed signals from **L-modes** and **ELMy H**-modes for both magnetic equilibria tested (EFIT and SCENE*))

- Different situation is for **ELM-free H-modes**. Neither EFIT or SCENE used in simulation produce adequate results.

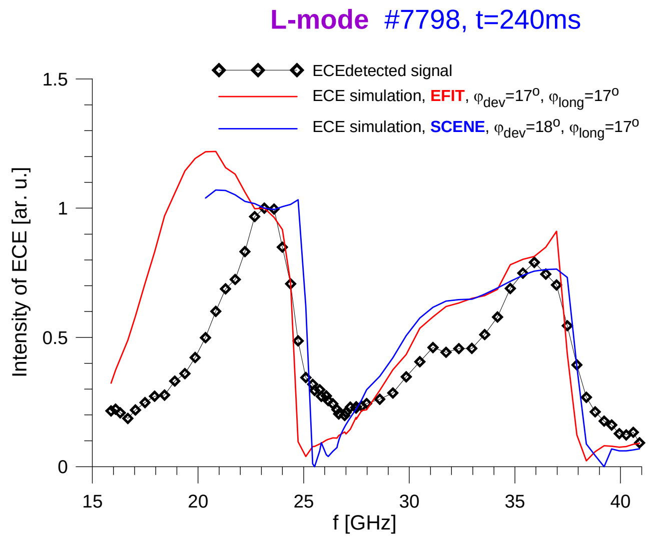

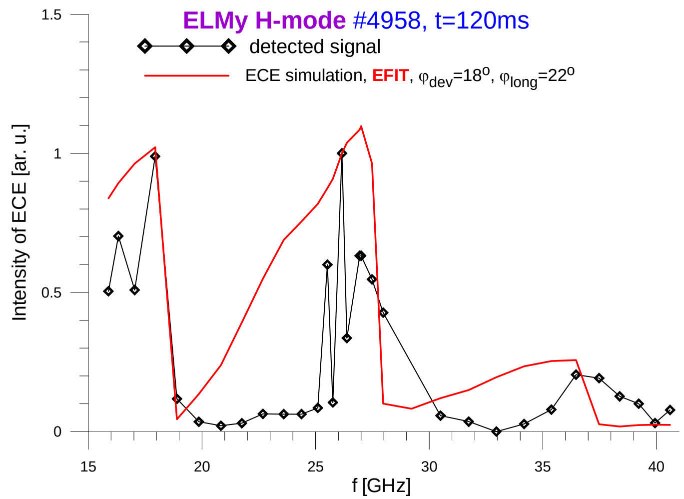

*) SCENE – Simulation of Self-Consistent Equilibria with Neoclassical Effects
H.R. Wilson: SCENE, UKAEA FUS 271 (1974), Culham, Abingdon, UK

EBW emission from ELM-free H-modes

Position of gaps in measured signal suggest that the magnetic field in the transport barrier is stronger than that predicted by EFIT and that it is non-monotonous (the position of the first gap is blurred by the turbulence in the conversion region which is placed in the SOL)

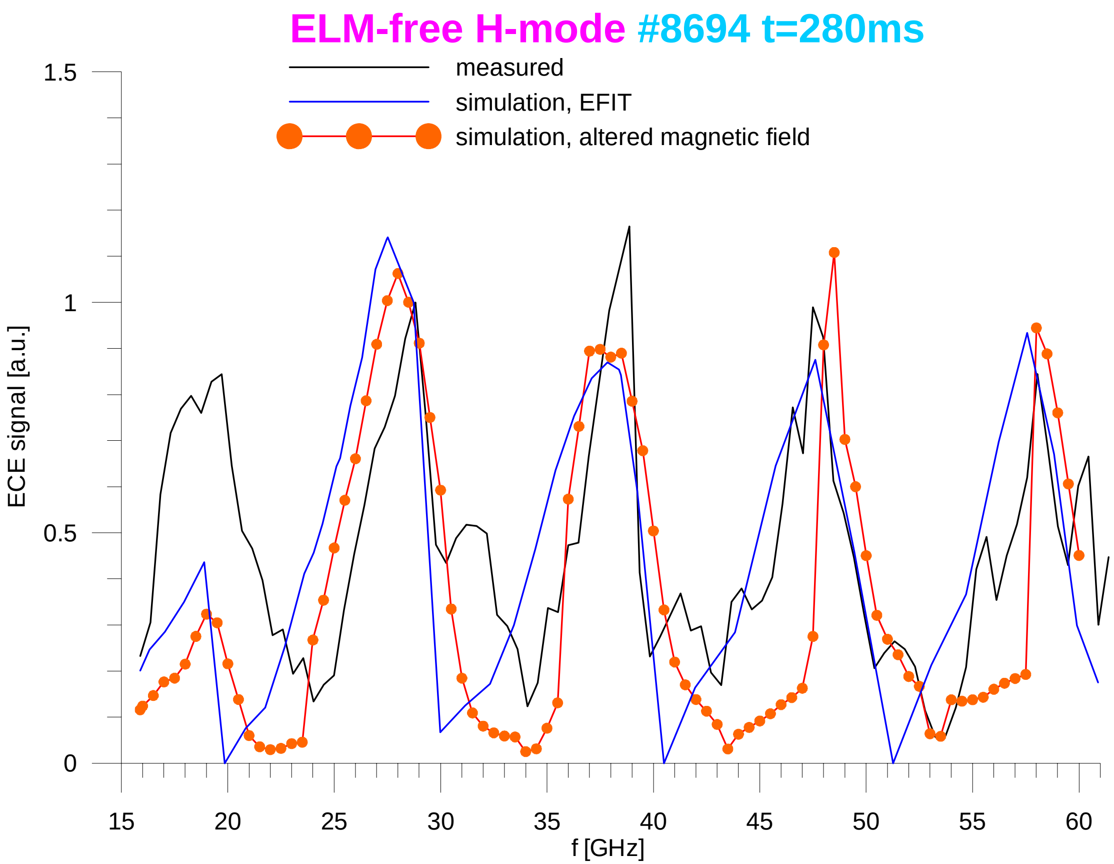

Reconstruction of magnetic field in the transport barrier from EBW signal in MAST

- The magnetic field at the n's gap $B(R_n)[T]=f_n[GHz]/28$ is given by the condition $nf_{ce}(R_n)=f_{UHR}(R_n)$
- We suppose that only the poloidal component ($B_{pol}=1/R d\psi/dR$) has a bump in the transport barrier , $B_R=0$ and B_{tor} has EFIT value (also B_Z out of TB). The shape of magnetic surfaces is adopted also from EFIT

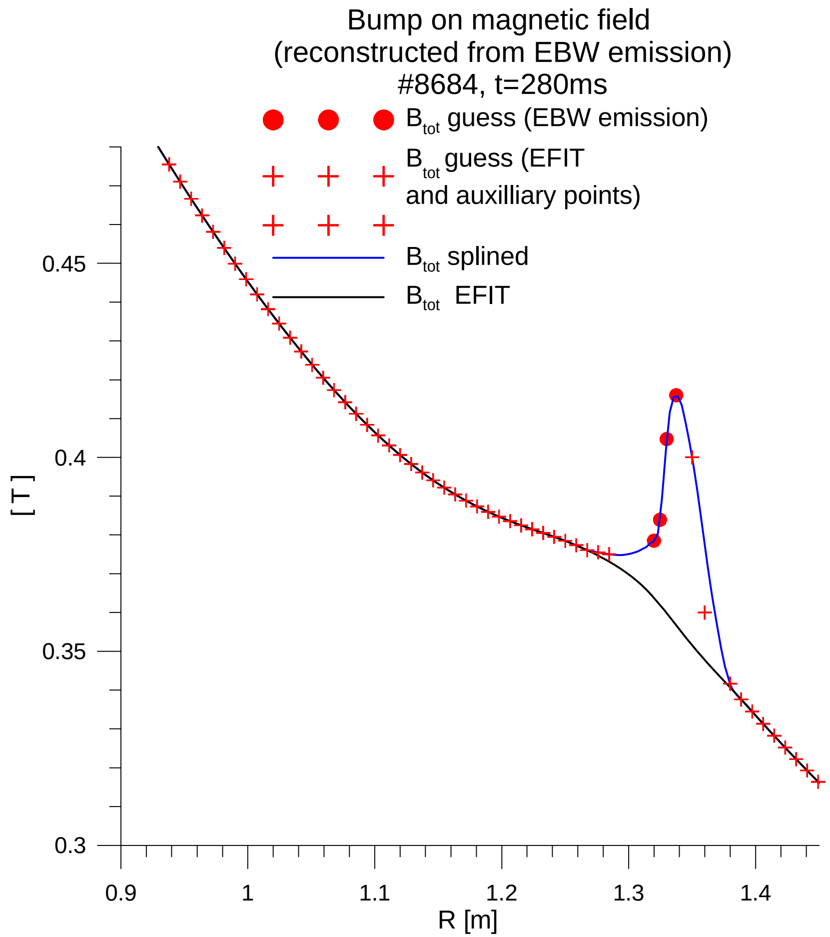

Magnetic field reconstructed from EBW emission in ELM-free H-modes and the structure of the transport barrier

From radial profile of the magnetic field in the equatorial plane we derive approximate magnetic surface equilibrium on the assumptions: $B_R=0$, $B_{tor}=B_{tor}(EFIT)$, $d\Psi(R)/dR=R*sqrt((B_{tot}(R))^2-(B_{tor}(R))^2)$, $\psi(R,Z)$ is determined by mapping EFIT values. As a consequence of bump on magnetic field profile, current double sheet appears in TB

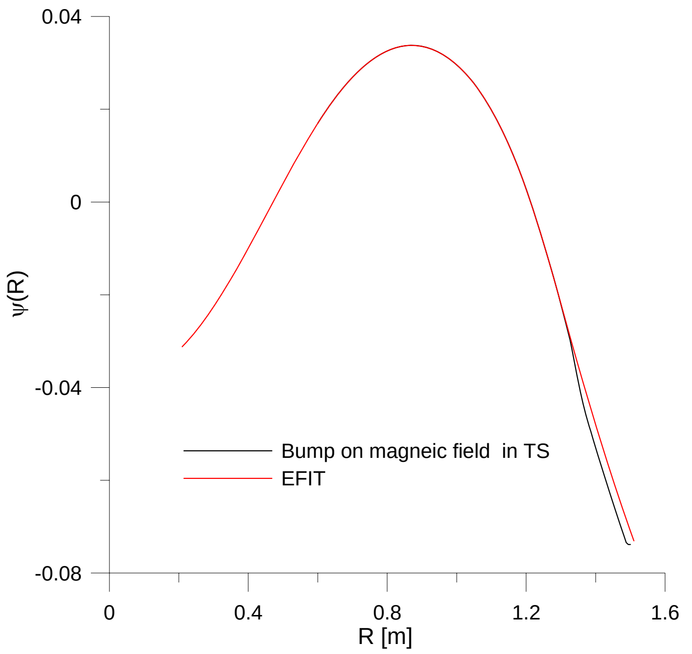

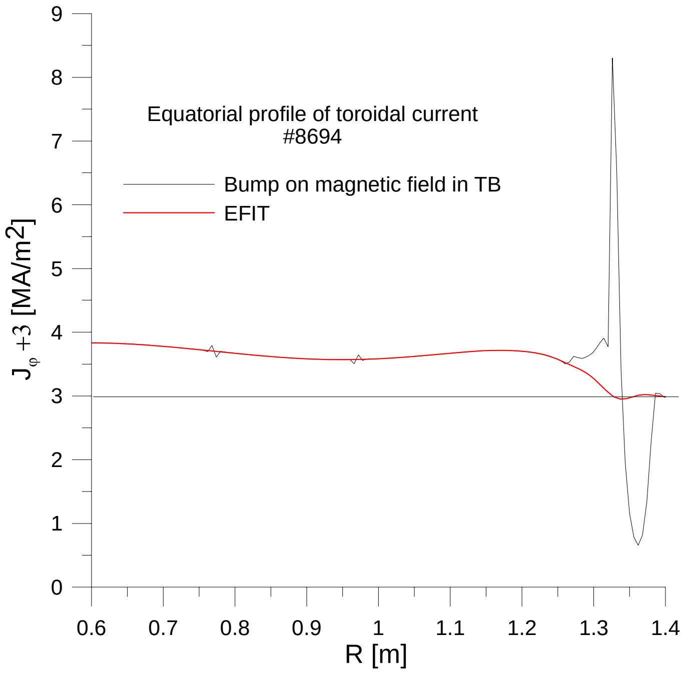

Effect of bump on the magnetic field in TB on EBW emission

- The position of peaks in EBW emission spectrum is determined by the window between top of bump at given harmonics and the bottom of absorption region of the higher harmonics. The position of peaks at higher harmonics is very sensitive to the magnitude of the magnetic field at the top of bump
- Broadening of is given by the factor

$$1/(1 \pm 3N_{\|}(v_T/c))$$

- In the shaded areas EBW are strongly damped and are emitted from the edges of these areas.
- EBW is emitted with $N_{\|}=1$ for $f<nf_{ce}$
- $N_{\|}$ oscillates for $f>nf_{ce}$ so here initial value of $N_{\|}$ was considered

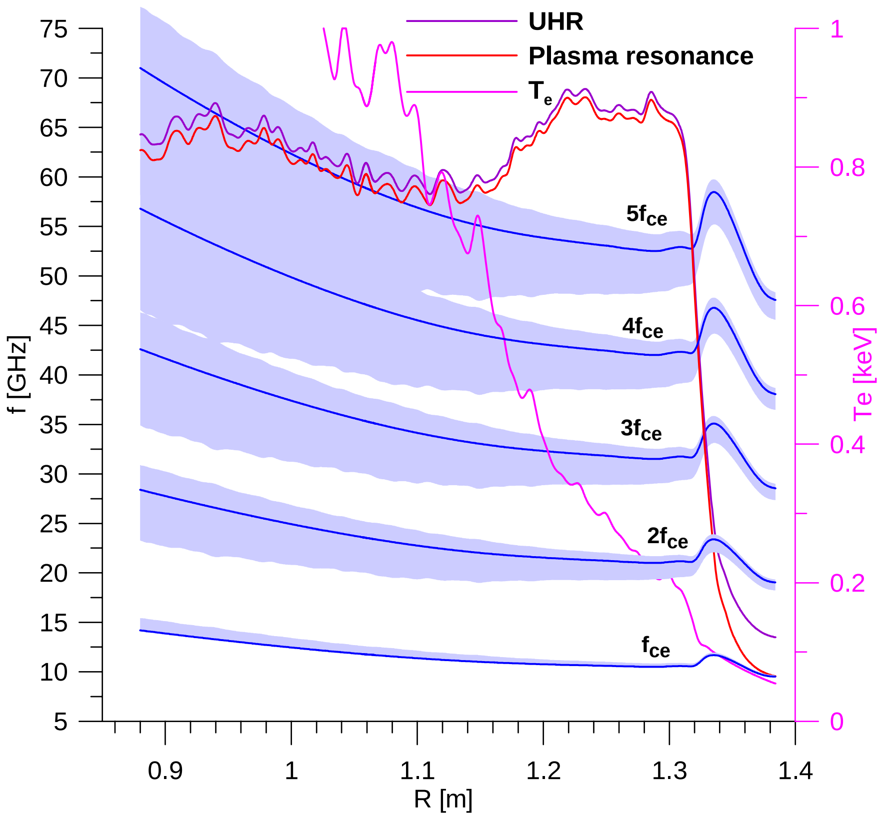

Magnetic bump induces the damping of EBW in rarefied plasma

- EBW emitted slightly above the third and higher harmonics is strongly reabsorbed in rarefied plasma in front of UHR
- the ray is launched from the UHR region and starts to propagate out of the plasma. Its frequency is approaching the 3rd electron cyclotron harmonic (magnetic field increases in this direction due to the bump) and it is partially absorbed here. The ray is then reverted back to the dense plasma and is fully absorbed at the 3rd harmonics at the plasma center. Emission is the reverse process and the ray emitted from the plasma center where plasma temperature is 1keV is partly reabsorbed at the plasma boundary so finally = 0.7keV. Waves with slightly lower frequency (e.g., 37GHz) are fully absorbed at the plasma boundary with = 0.1keV only.

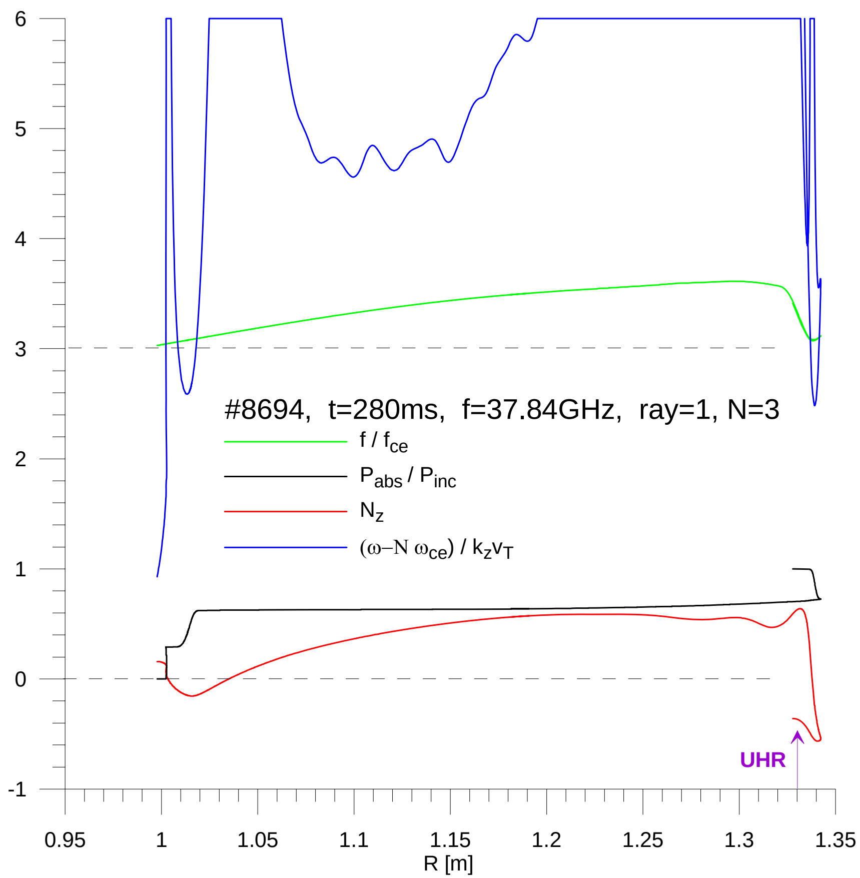

Time development of the plasma temperature in NSTX

- We reach excellent fit between simulated and the EBW signal detected by NSTX (EBW signal is noisy due to fluctuation of density in the conversion region – no fluctuation are included in the simulation)
- Time development central temperature is determined from reading of 16.5GHz signal

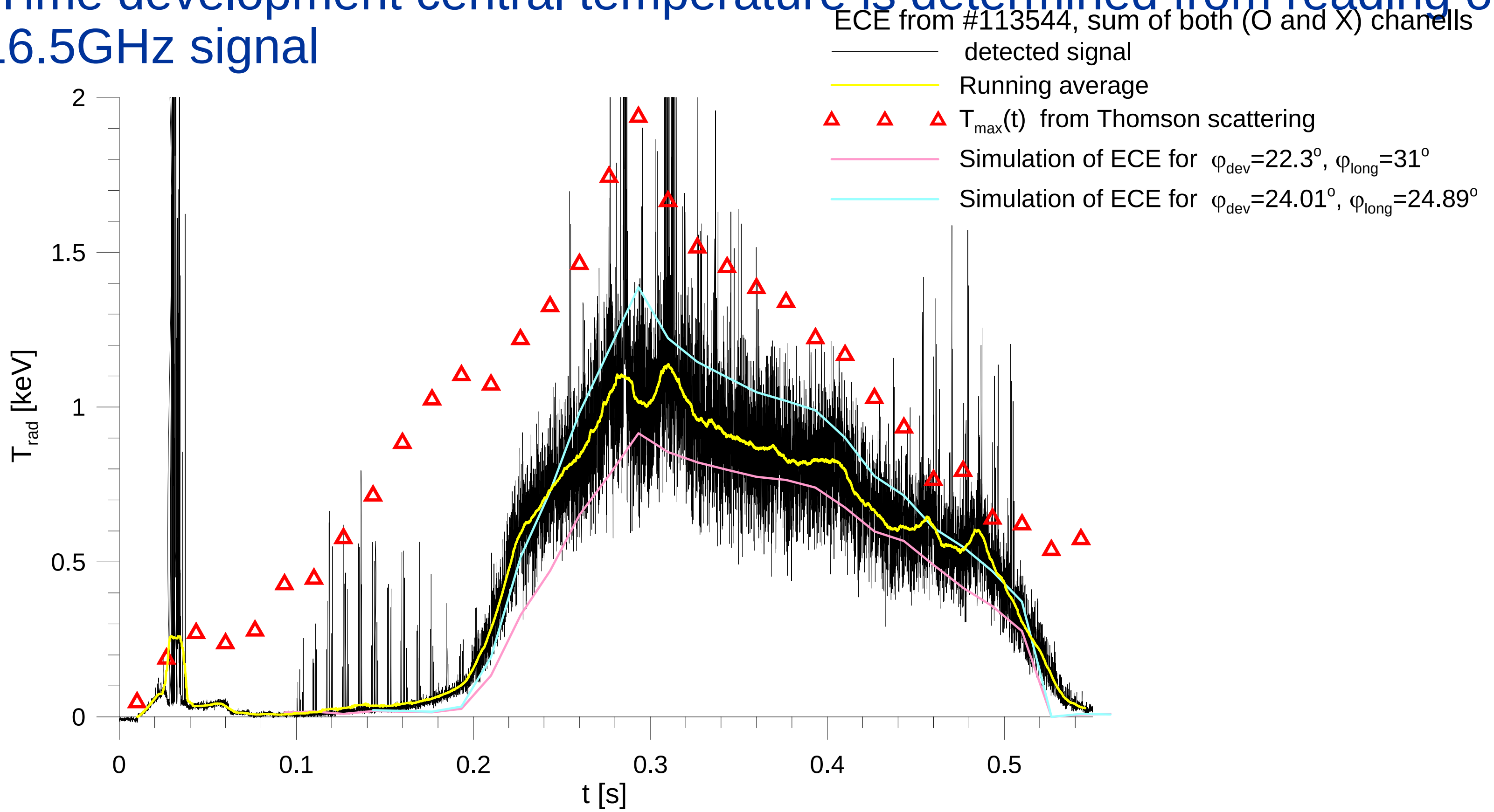

Antenna orientation and the EBW-X-O conversion efficiency

Contour map of conversion efficiency projected to the waist for O-polarization. #113544, t=0.325, f=16.5GHz

Actual antenna orientation ($\varphi_{dev} = 23.3^{o}, \varphi_{long} = 31^{o}$) is not optimal

Optimum antenna orientation $\varphi_{dev} = 24.01^{o}, \varphi_{long} = 24.89^{o}$

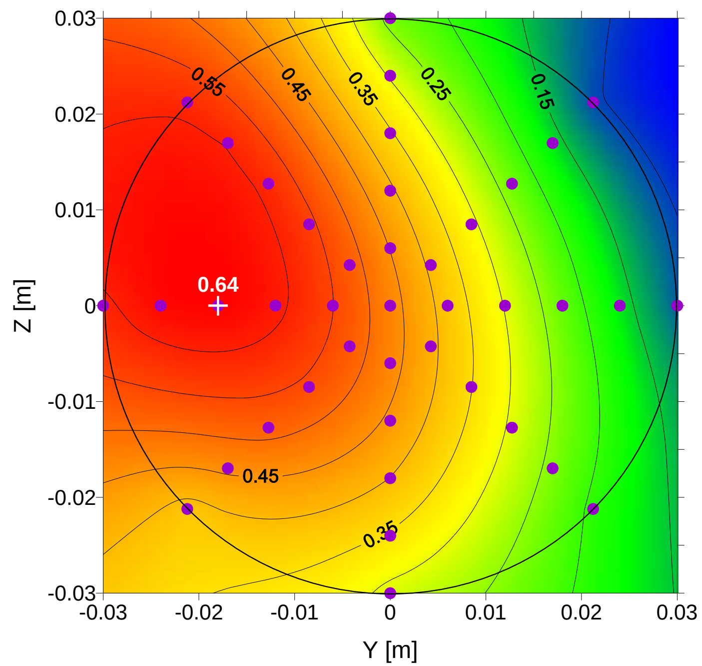

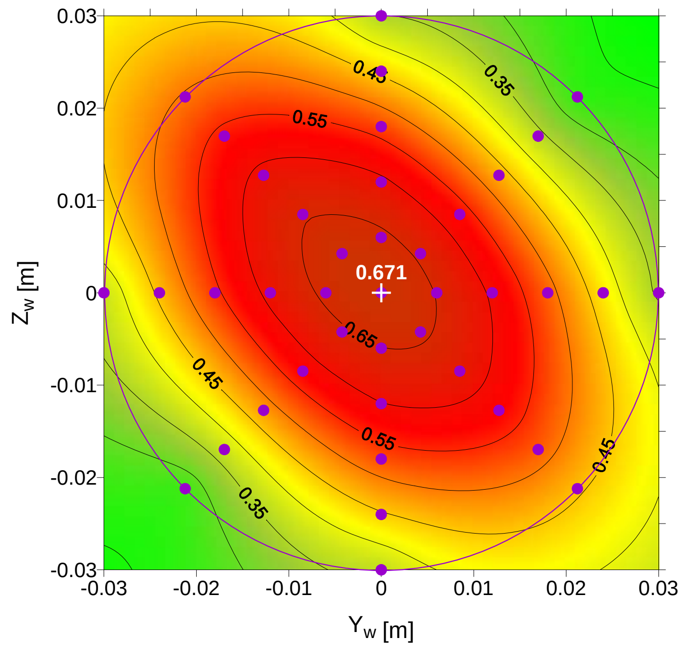

Initial stage of discharge

- For 0< t<0.3 EBW signal at 16.5GHz cannot be used for determination of the central temperature. EBW is emitted from the second harmonics form plasma surface

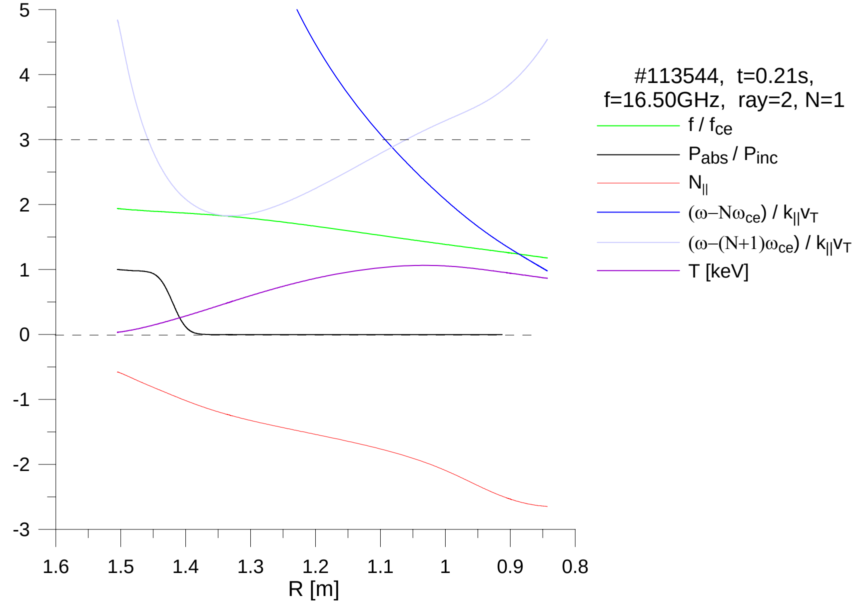

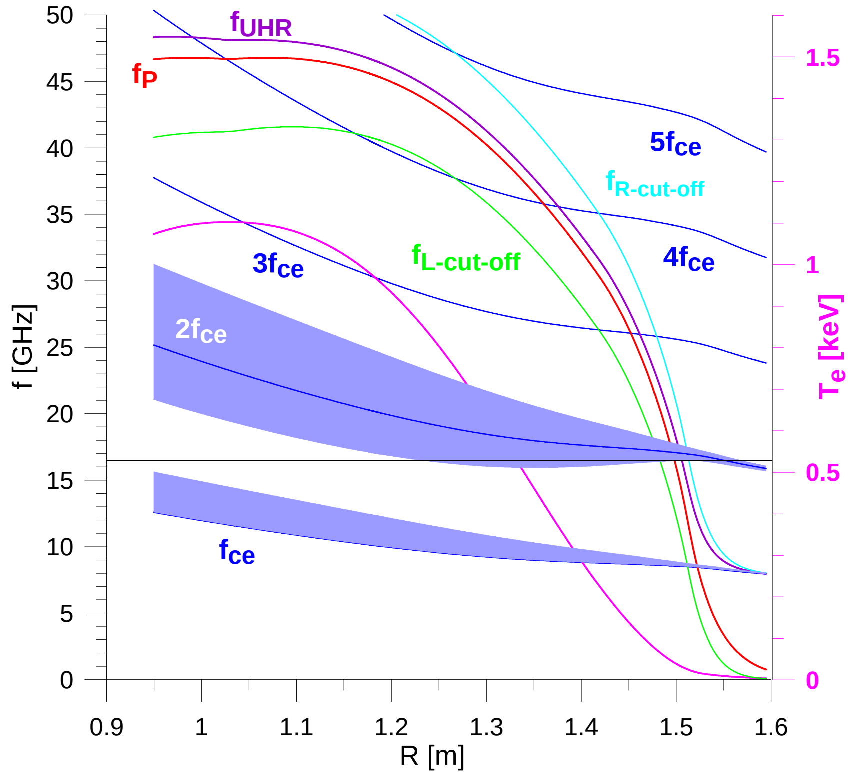

Time development of EBW-X-O conversion efficiency

- Conversion efficiency is practically constant during the central part of discharge

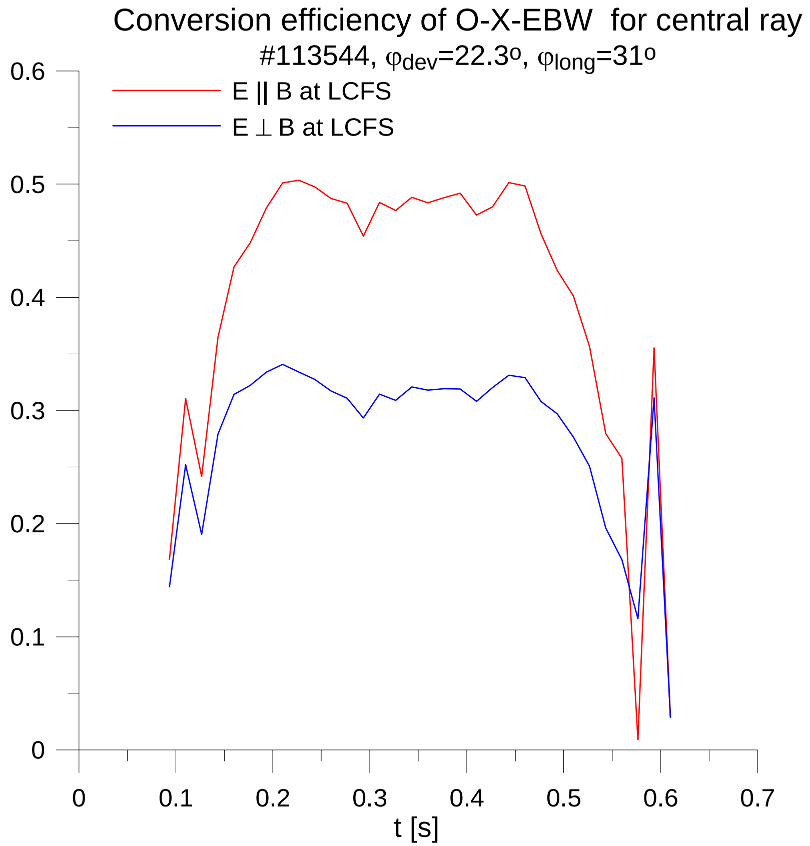

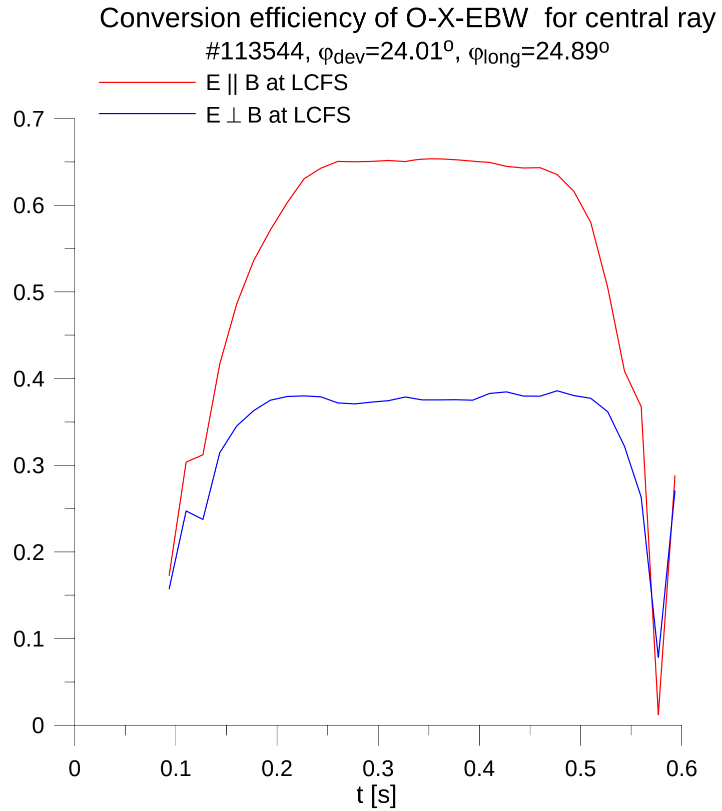

Simulation of time development of EBW emission from O and X channels

- Detected O-polarized wave fit exactly with its simulation
- Simulated X-polarized wave is slightly weaker

O-channel EBW from #113544 **X-channel**

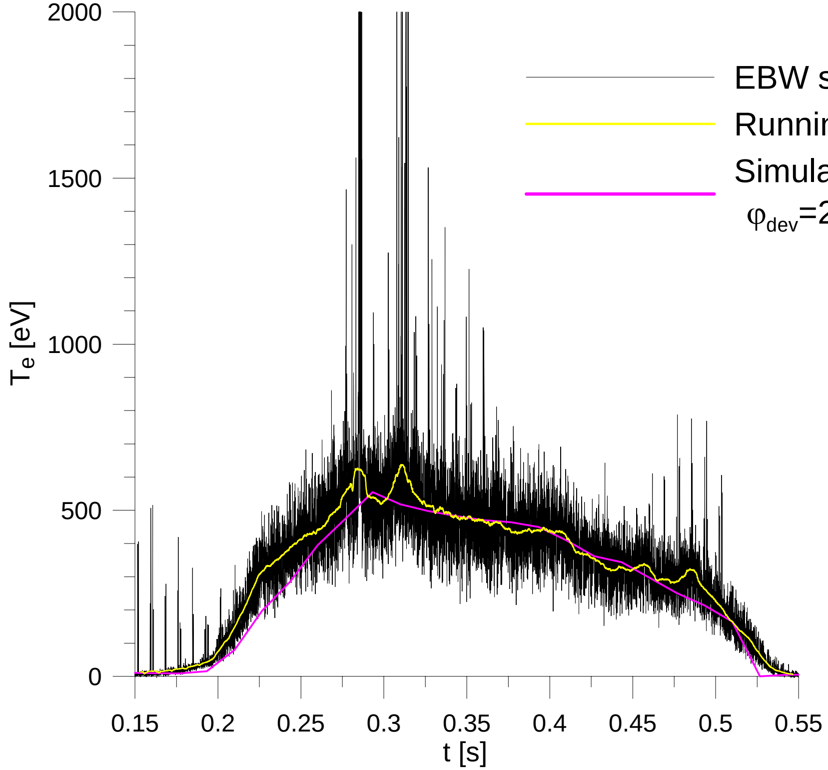

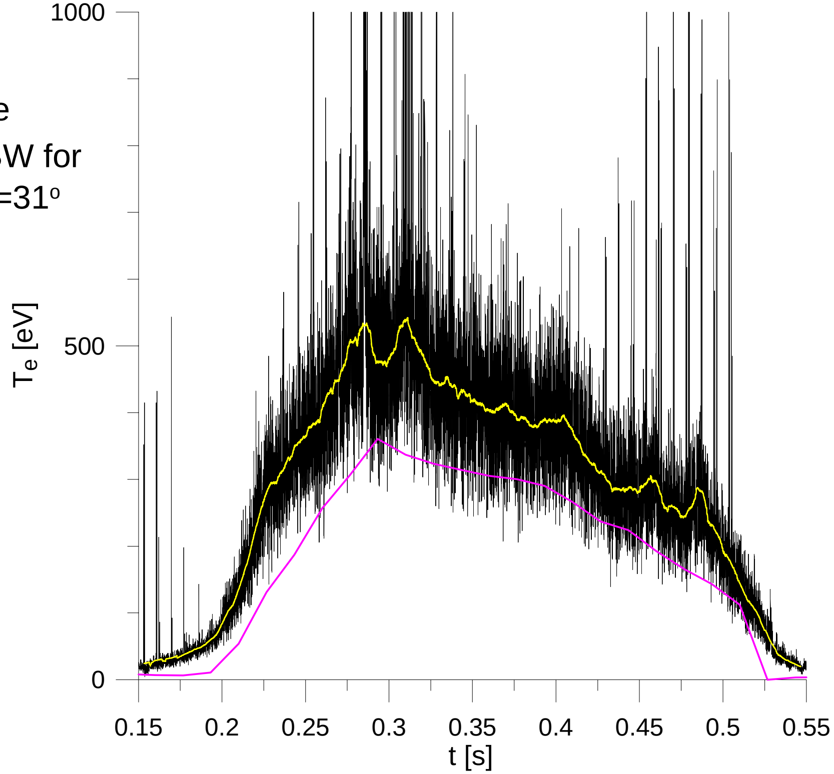

Comparison central temperature measured by Thomson scattering and deduced from EBW signal

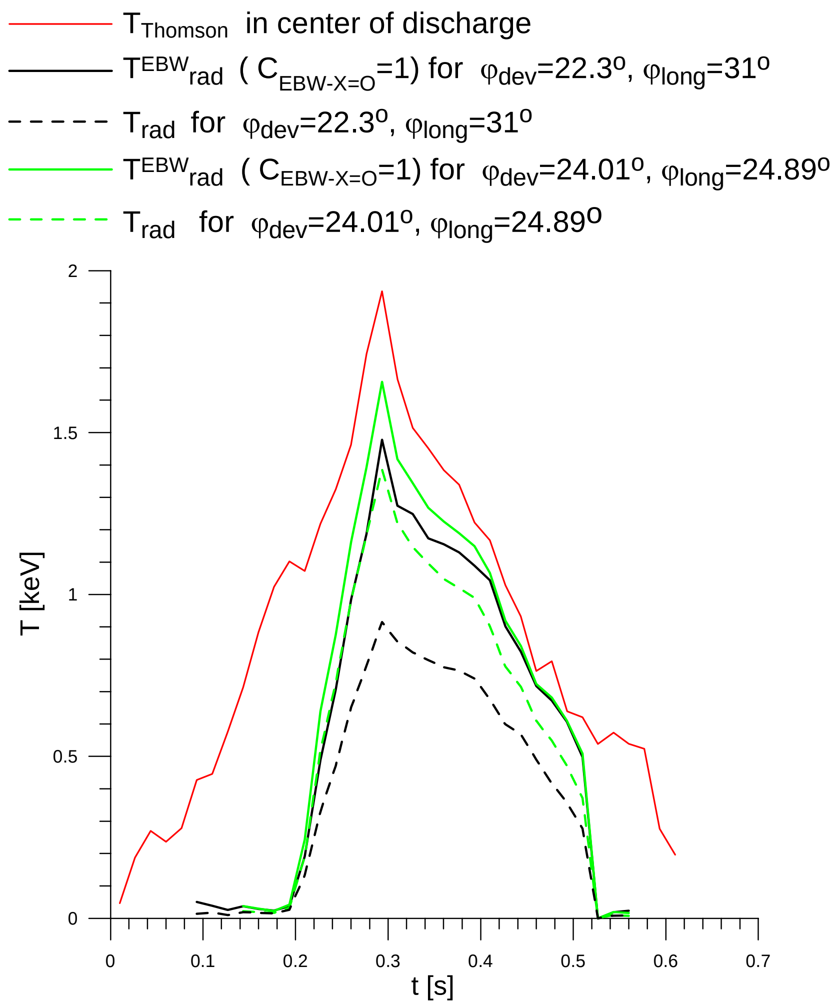

- EBW temperature is always less than the actual temperature
- Even ideal effective temperature of EBW radiation for conversion efficiency equal 1 is smaller then $T_{Thomson}$ because of reabsoption of EBW and the parasitic radiation from the second harmonic
- T_{rad} is father reduced by imperfect conversion
- This last effect is more pronounced if the antenna does not have optimum orientation

CONCLUSIONS

Current theoretical model incorporates nearly all the details of the MAST EBW antenna and plasma model based on experimental data.

For ELM-free H-mode in MAST, simulation based on EFIT equilibrium suggest the the magnetic filed in TB is too weak. We obtain better fit between EBW emission and the simulation when the last was based on reconstructed magnetic field (bump in TB). At present we have no selfconsistent solution of magnetic equilibrium and the origin of the double current sheet in TB is unsolved

We obtain the excellent fit between time development of the central temperature in NSTX determined from the EBW emission detected at 16.5GHz and its simulation. We show that the conversion efficiency of EBW-X-O process is constant during the main part of discharge. We also show that the temperature determined at the optimum orientation of antenna will be near the temperature determined from Thomson scattering.

EBW emission from ELM-free H-modes

- Position of gaps in measured signal suggest that the magnetic field in the transport barrier is stronger than that predicted by EFIT and that it is non-monotonous

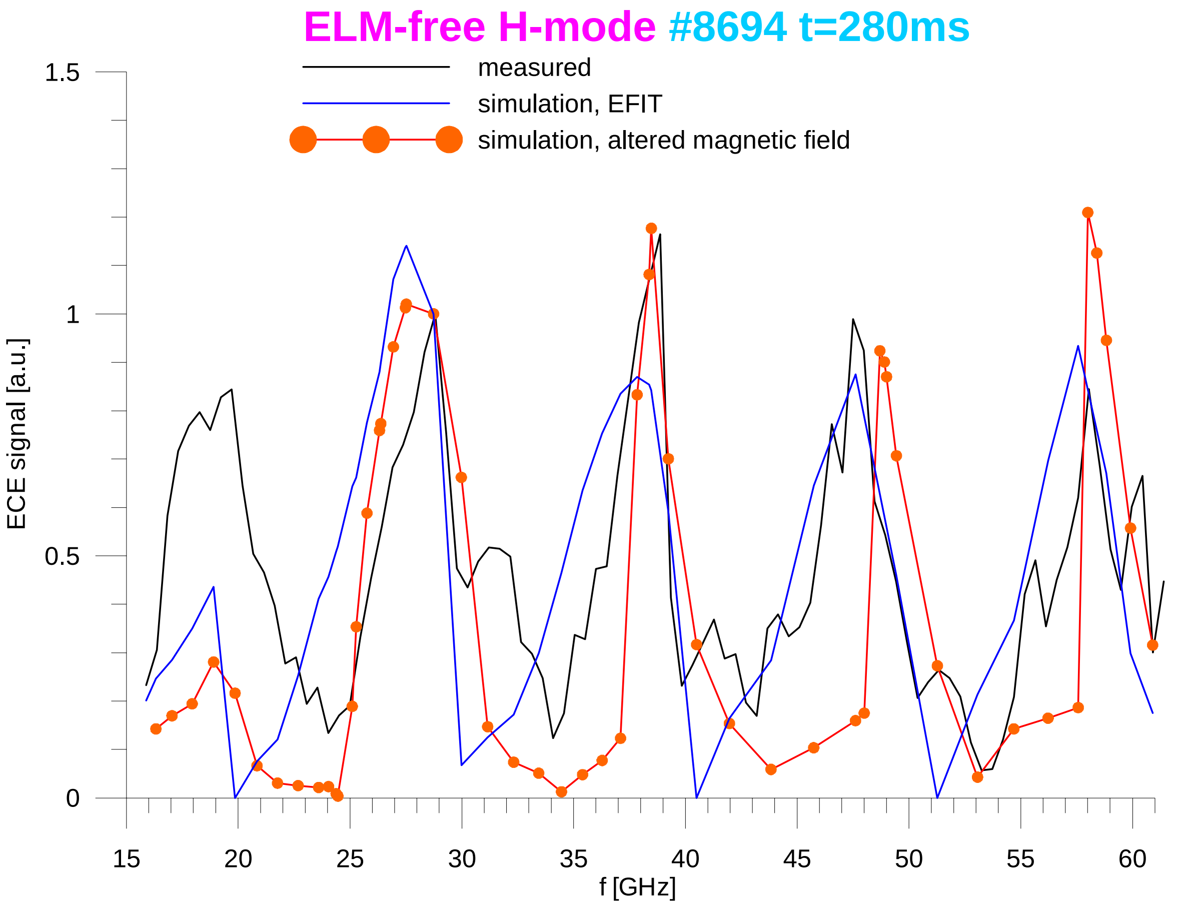

Reconstruction of magnetic field in the transport barrier from EBW signal in MAST

- The magnetic field at the n's gap $B(R_n)[T]=f_n[GHz]/28$ is given by the condition $nf_{ce}(R_n)=f_{UHR}(R_n)$
- We suppose that only the poloidal component ($B_{pol}=1/Rd\psi/dR$) has a bump in the transport barrier , $B_R=0$ and B_{tor} has EFIT value (also B_Z out of TB). The shape of magnetic surfaces is adopted also from EFIT

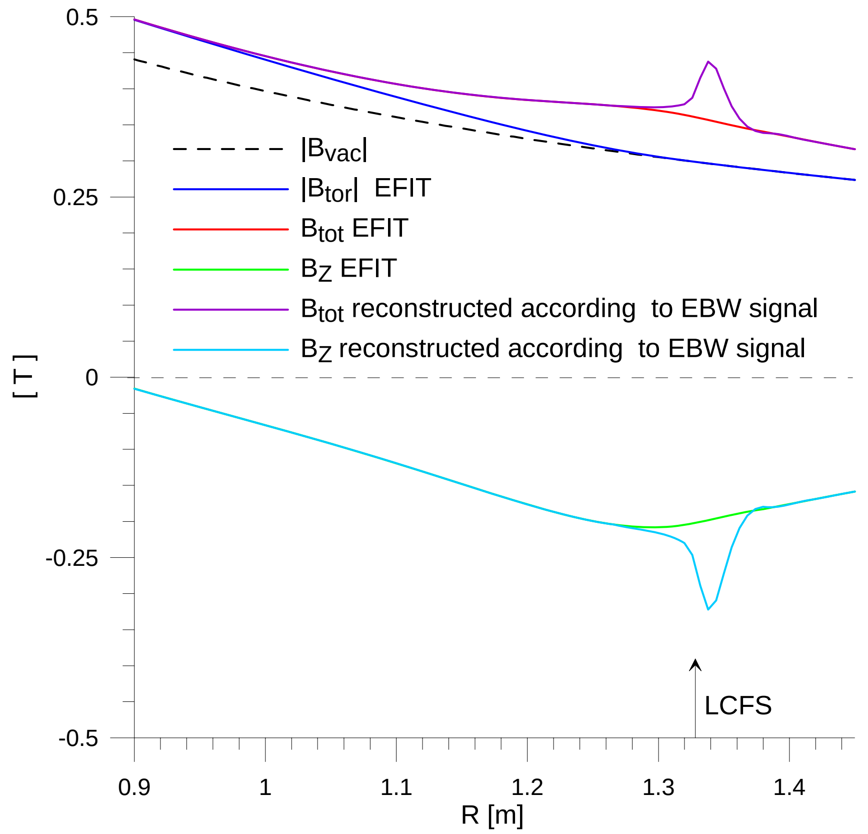

Effect of bump on the magnetic field in TB on EBW emission

- This effect can be seen from radial profiles of the characteristic resonances
- Broadening of is given by the factor
  $$1/(1 \pm 3N_{||}(v_T / c))$$
- Rays with frequency below nf_{ce} are usually emitted with $N_{||}$=1
- $N_{||}$ oscillates for rays with frequency above nf_{ce} so here initial value of $N_{||}$ was considered.
- In the shaded areas EBW are strongly damped and are emitted from the edges of these areas.
- The broadening of gaps in the emitted spectrum is caused by the bump on the magnetic field in the transport barrier. For two first harmonics the magnetic field decreases in the transport barrier from UHR region in the direction into the plasma center. EBW with frequency slightly below are than emitted from the boundary cold plasma.

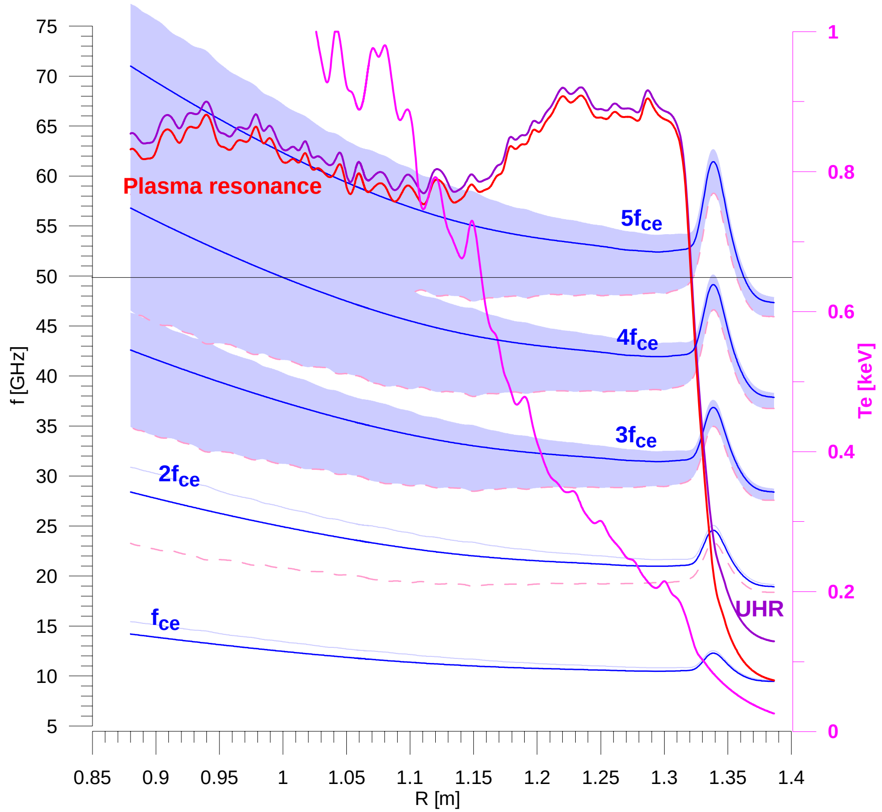

Adaptive method convergence properties

- Typical error dependence of the global and local error are shown for $\nu/f=0.001$
- For common precision requirements (0.005-0.001) the method is fast
- The error estimates correspond with each other

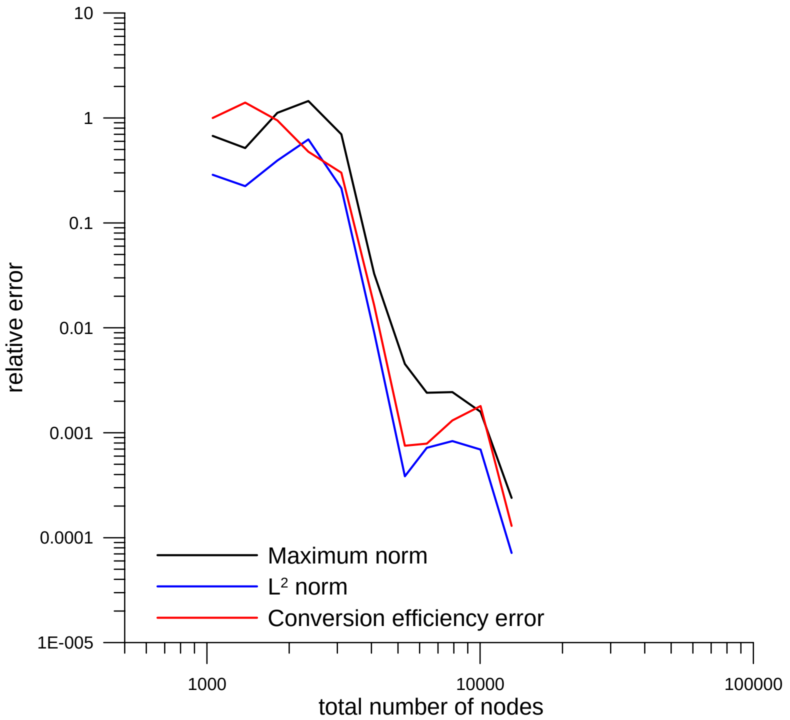

Dependence of various global error estimates on the total number of nodes

the error decreases approx. as $\sim n^{-4.5}$

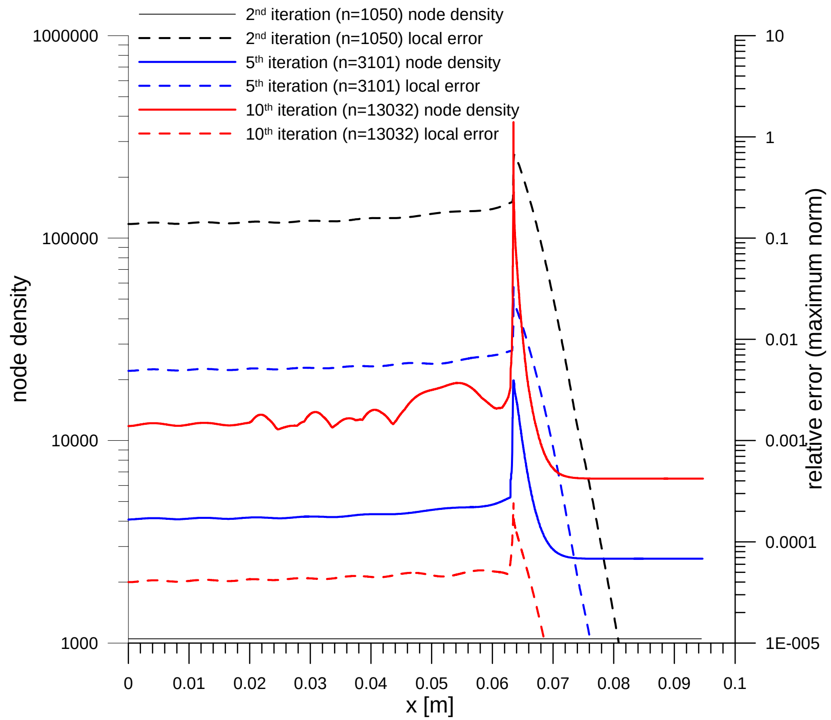

Evolution of local error and node density with mesh refinement